

Quantifying Distributions of Lyman Continuum Escape Fraction

Renyue Cen¹ and Taysun Kimm²

ABSTRACT

Simulations have indicated that most of the escaped Lyman continuum photons escape through a minority of solid angles with near complete transparency, with the remaining majority of the solid angles largely opaque, resulting in a very broad and skewed probability distribution function (PDF) of the escape fraction when viewed at different angles. Thus, the escape fraction of Lyman continuum photons of a galaxy observed along a line of sight merely represents the properties of the interstellar medium along that line of sight, which may be an ill-representation of true escape fraction of the galaxy averaged over its full sky. Here we study how Lyman continuum photons escape from galaxies at $z = 4 - 6$, utilizing high-resolution large-scale cosmological radiation-hydrodynamic simulations. We compute the PDF of the mean escape fraction ($\langle f_{\text{esc,1D}} \rangle$) averaged over mock observational samples, as a function of the sample size, compared to the true mean (had you an infinite sample size). We find that, when the sample size is small, the apparent mean skews to the low end. For example, for a true mean of 6.7%, an observational sample of (2,10,50) galaxies at $z = 4$ would have have 2.5% probability of obtaining the sample mean lower than $\langle f_{\text{esc,1D}} \rangle = (0.007\%, 1.8\%, 4.1\%)$ and 2.5% probability of obtaining the sample mean being greater than (43%, 18%, 11%). Our simulations suggest that at least ~ 100 galaxies should be stacked in order to constrain the true escape fraction within 20% uncertainty.

1. Introduction

A fraction of the Lyman continuum (LyC) photons generated by young massive stars is believed to escape from the host galaxies to enter the intergalactic space. This is a fundamental quantity to determine the epoch and pace of cosmological reionization, provided that the universe is reionized by stars (e.g., Gnedin 2000; Cen 2003). After the completion of cosmological reionization, it plays another important role in determining the ultra-violet (UV) radiation background (on both sides of the Lyman limit) in conjunction with another major source of UV photons - quasars - that progressively gains importance at lower redshift (e.g., Faucher-Giguère et al. 2008; Fontanot et al. 2014).

Observations of star-forming galaxies at high redshifts ($z \sim 3$) suggest a wide range of the escape fraction of ionizing photons. While only a small fraction of LyC photons (\lesssim a few percent) escapes from their host galaxies in the majority of the Lyman break galaxy samples, a non-negligible

¹Princeton University Observatory, Princeton, NJ 08544; cen@astro.princeton.edu

²Princeton University Observatory, Princeton, NJ 08544; kimm@astro.princeton.edu

number of them ($\sim 10\%$) shows high levels of LyC flux corresponding to $\langle f_{\text{esc},1\text{D}} \rangle \sim 10\%$ (Shapley et al. 2006; Iwata et al. 2009; Nestor et al. 2011, 2013; Mostardi et al. 2013). Cooke et al. (2014) claim that the mean escape fraction may be even higher ($\langle f_{\text{esc},1\text{D}} \rangle \sim 16\%$) if the observational sample is not biased toward the galaxies with a strong Lyman limit break. It is not well understood quantitatively, however, what the probability distribution function (PDF) of the LyC escape fraction is and how a limited observational sample size with individually measured escape fractions can be properly interpreted, because of both possible large variations of the escape fraction from sightline to sightline for a given galaxy and possible large variations from galaxy to galaxy. The purpose of this *Letter* is to quantify how LyC photons escape, in order to provide a useful framework for interpreting and understanding the true photon escape fraction given limited observational sample sizes.

2. Simulations

To investigate how LyC photons escape from their host halos, we make use of the cosmological radiation hydrodynamic simulation performed using the Eulerian adaptive mesh refinement code, RAMSES (Teyssier 2002; Rosdahl et al. 2013, ver. 3.07). The reader is referred to Kimm & Cen (2014, the FRU run) for details, where a detailed prescription for a new, greatly improved treatment of stellar feedback in the form of supernova explosion is given. Specifically, the new feedback model follows the dynamics of the explosion blast waves that capture the solution for all phases (from early free expansion to late snowplow), independent of simulation resolution and allow for anisotropic propagation.

The initial condition for the simulation is generated using the MUSIC software (Hahn & Abel 2011), with the WMAP7 parameters (Komatsu et al. 2011): $(\Omega_{\text{m}}, \Omega_{\Lambda}, \Omega_{\text{b}}, h, \sigma_8, n_s = 0.272, 0.728, 0.045, 0.702, 0.82, 0.96)$. We adopt a large volume of $(25\text{Mpc}/h)^3$ (comoving) to include the effect of large-scale tidal fields on the galaxy assembly. The entire box is covered with 256^3 root grids, and high-resolution dark matter particles of mass $M_{\text{dm}} = 1.6 \times 10^5 M_{\odot}$ are employed in the zoomed-in region of $3.8 \times 4.8 \times 9.6 \text{ Mpc}^3$. We allow for 12 more levels of grid refinement based on the density and mass enclosed within a cell in the zoomed-in region to have a maximum spatial resolution of 4.2 pc (physical). Star formation is modeled by creating normal and runaway particles in a dense cell ($n_{\text{H}} \geq 100 \text{ cm}^{-3}$) with the convergent flow condition (Kimm & Cen 2014, the FRU run). The minimum mass of a normal (runaway) star particle is $34.2 M_{\odot}$ ($14.6 M_{\odot}$). We use the mean frequency of Type II supernova explosions of $0.02 M_{\odot}^{-1}$, assuming the Chabrier initial mass function. Dark matter halos are identified using the HaloMaker (Tweed et al. 2009).

Eight consecutive snapshots are analyzed at each redshift ($3.96 \leq z \leq 4.00$, $4.92 \leq z \leq 5.12$, and $5.91 \leq z \leq 6.00$) to increase the sample size in our calculations. At each snapshot there are ≈ 142 , 137, and 104 halos in the halo mass range of $10^9 \leq M_{\text{vir}} < 10^{10} M_{\odot}$, and 15, 10, and 7 halos with mass $M_{\text{vir}} \geq 10^{10} M_{\odot}$. The most massive galaxy at $z = 4$ (5, 6) has stellar mass of $1.6 \times 10^9 M_{\odot}$ (6.0×10^8 , $2.5 \times 10^7 M_{\odot}$), and host halo mass $8.8 \times 10^{10} M_{\odot}$ (5.2×10^{10} , $4.1 \times 10^{11} M_{\odot}$)

The escape fraction is computed as follows. We cast 768 rays per star particle and follow their

propagation through the galaxy. Each ray carries the spectral energy distribution (SED), including its LyC emission, determined using STURBURST99 (Leitherer et al. 1999), given the age, metallicity, and mass of the star particle. The LyC photons are attenuated by neutral hydrogen (Osterbrock & Ferland 2006) and SMC-type dust (Draine et al. 2007) in the process of propagation. For a conservative estimate, we assume the dust-to-metal ratio of 0.4. We also simply assume that dust is destroyed in hot gas ($T > 10^6$ K). We note that attenuation due to dust is only significant in the most massive galaxy ($M_{\text{star}} = 1.1 \times 10^9 M_{\odot}$, $\tau_d = 0.58$) in our sample. The second most massive galaxy ($M_{\text{star}} = 3.6 \times 10^8 M_{\odot}$) shows $\tau_d = 0.29$, meaning that it reduces the number of photons by only $< 30\%$. Given that the dust-to-metal ratio is even smaller than 0.4 in low-metallicity systems (Lisenfeld & Ferrara 1998; Engelbracht et al. 2008; Galametz et al. 2011; Fisher et al. 2013), it is likely that the attenuation by dust is even less significant in our simulated galaxies. We define the true escape fraction of the galaxy as the ratio of the sum of all outward fluxes at the virial sphere to the sum of the initially emitted fluxes of all stellar particles in the galaxy; we shall call this $f_{\text{esc},3\text{D}}$. In addition, an observer at infinity at a random point in the sky of the galaxy collects all LyC fluxes and defines the escape fraction along that particular line of sight; this is called $f_{\text{esc},1\text{D}}$.

3. Probability Distribution Functions of LyC Photon Escape Fraction

It is useful to give a qualitative visual illustration of how LyC photons may escape from galaxies at $z = 4$. Figure 1 shows three examples of an all-sky map - the sky an observer sitting at the center of the galaxy would see - of the neutral hydrogen column density. We note that 8 dex of dynamical range is plotted and recall that at the Lyman limit a neutral hydrogen column density of $\sim 10^{17} \text{cm}^{-2}$ would provide an optical depth of ~ 1 . As a result, LyC photons can only escape through highly ionized or evacuated “holes” indicated by dark blue colors on the maps and the transition from near transparency to very opaque is fast. This indicates that the escaping LyC photons are dominated by those that escape through completely unobscured channels and the amount of escaped LyC photons for a given galaxy depends strongly on the direction. Moreover, it is evident that, in addition to large variations from position to position on the sky for a given galaxy, there are large variations of the overall column density structures from galaxy to galaxy. For example, the galaxy in the top-left panel shows no transparent sky patches at all, which is typical for galaxies during times of intense starburst as shown in Kimm & Cen (Figure 4 2014). On the other hand, the galaxy in the bottom panel has large swaths of connected transparent patches that cover nearly one half of the sky, typical for galaxies at periods following the blowout of gas subsequent to intense starburst (Figure 4 Kimm & Cen 2014). This qualitative behavior is also found earlier in independent simulations by Wise & Cen (2009).

Let us now turn to more quantitative results. Figure 2 shows the probability distribution of the apparent escape fraction for massive halos (top) and less massive halos (bottom) at $z = 4$ (left column) and $z = 6$ (right column). Black histograms show the distribution of the true (3D) escape fraction of each sample (i.e., from the viewpoint of the overall intergalactic medium), while red histograms show the PDF of the apparent escape fraction (i.e., from the point of view of observers placed at a far distance). Note that the distribution of the true escape fraction is noisier than that of

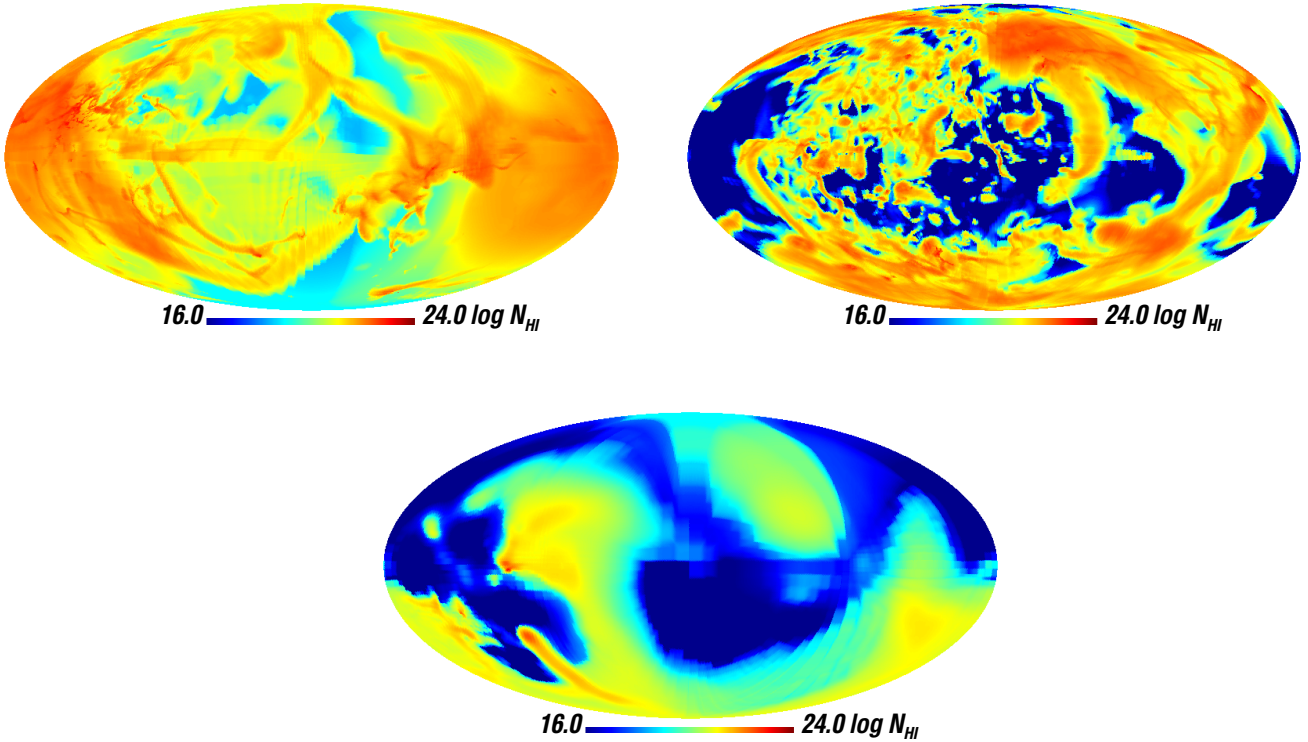


Fig. 1.— shows three examples of all-sky maps - the sky an observer sitting at the center of the galaxy would see - of the neutral hydrogen for most massive ($M_{vir} = 7.8 \times 10^{10} M_{\odot}$, top left panel), second massive ($6.1 \times 10^{10} M_{\odot}$, top right panel), and a smaller halo ($1.8 \times 10^9 M_{\odot}$, bottom). The observer is placed at the center of the halo. Note that the actual escape fraction presented later is computed by ray-tracing LyC photons of all stellar particles spatially distributed through the clumpy interstellar medium until escaping through the virial sphere. The true escape fraction of LyC photons of these halos are 5.4%, 12%, and 5.0%, respectively.

the apparent escape fraction due to the smaller sample size for the former, because for (3D) escape fraction each galaxy is counted once but for the apparent escape fraction each galaxy is sampled many times. In terms of the mean escape fraction, there is a trend that, at a given redshift, the galaxies embedded in more massive halos tend to have a lower mean escape fraction.

There is also a weak trend that the escape fraction increases with redshift. For example, the true (3D) median escape fractions are (7.0%, 9.5%) for the halos of masses ($\geq 10^{10}, 10^9 - 10^{10}$) M_{\odot} , respectively, at $z = 4$; the true (3D) median escape fractions are (8.8%, 29%) for the halos of masses ($\geq 10^{10}, 10^9 - 10^{10}$) M_{\odot} , respectively, at $z = 6$. Upon a close examination we suggest that the redshift dependence can be attributed, in part, to the following findings. At a given halo mass, the specific star formation rate decreases with decreasing redshifts at $4 \leq z \leq 6$. As star formation becomes less episodic at lower redshifts, it takes longer to blow out the star-forming clouds via SNe. Consequently, a larger fraction of LyC photons is absorbed by their birth clouds. We also find that the specific star formation rate does not change notably at $z > 6$ while the mean density

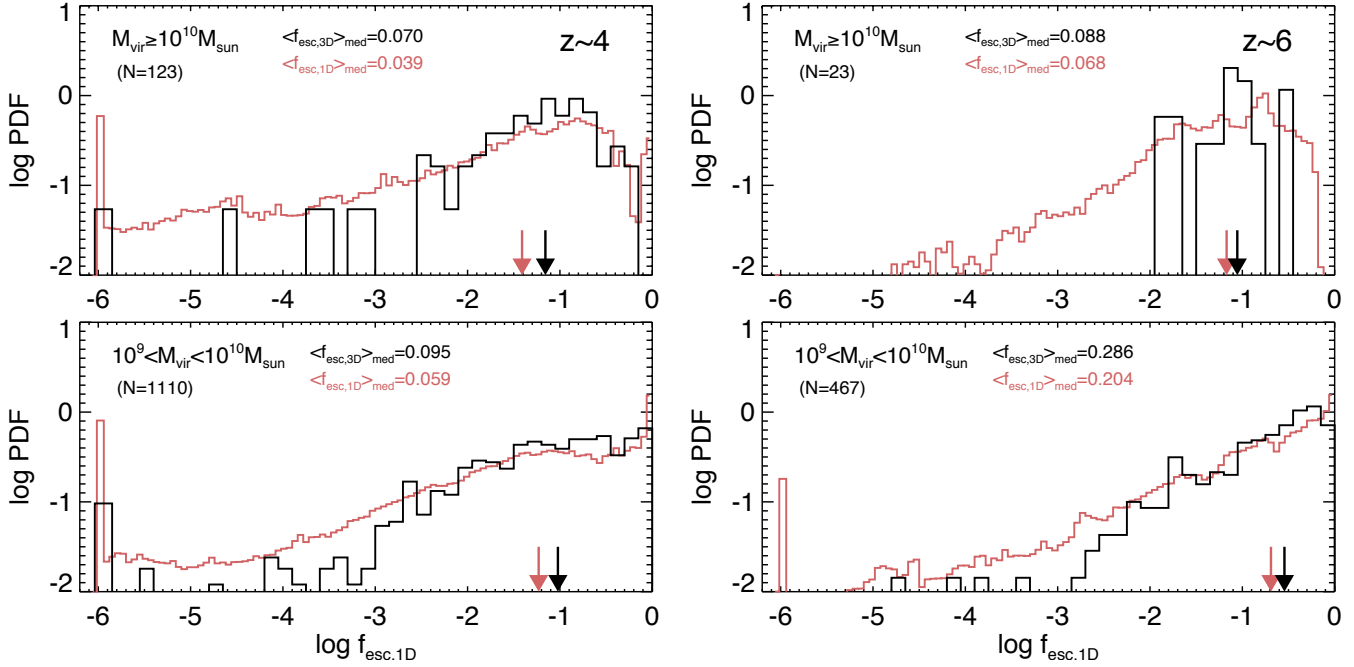


Fig. 2.— shows the probability distribution of the apparent escape fraction for massive halos (top panel) and less massive halos (bottom panel) for $z = 4$ (left column) and $z = 6$ (right column). Black histograms show the distribution of the true escape fraction of each sample, while red histograms show the PDF of the apparent escape fraction. The median of the distribution is shown as arrows.

of the halo increases with redshifts, explaining an opposite trend found in Kimm & Cen (2014) at $7 \leq z \leq 11$. The predicted median escape fraction for halos with $10^9 \leq M_{\text{halo}} \leq 10^{11} M_{\odot}$ at $4 \leq z \leq 6$ is generally smaller than the previous studies (10 – 30% Razoumov & Sommer-Larsen 2010; Yajima et al. 2014), although the trend at $z < 6$ is broadly consistent with Razoumov & Sommer-Larsen (2010). Nevertheless, it is prudent to bear in mind that the sometimes conflicting results and trends among studies with respect to redshift may be in part due to still limited galaxy sample sizes.

Figure 3 is similar to Figure 2, except the galaxy sample is subdivided according to their star formation rates (SFRs). We note that this division according to SFRs introduces subtle degeneracies. For example, a lower SFR does not necessarily correspond to a less massive galaxy; instead, a lower SFR may correspond to the phase of a galaxy between two star formation bursts. The significantly higher escape fraction for the lowest SFR bin (bottom panels) is, to the most part, due to a post-starburst phase when the interstellar medium has been cleared out by the preceding burst and SFR has abated, as noted in Kimm & Cen (2014). Thus, if we do not consider the lowest SFR bin, it seems that the mean escape fraction does not strongly depend on SFR at $z = 4 - 6$. The escape fraction from the most actively star-forming galaxy sample with $0.3 < \text{SFR} < 10 M_{\odot}/\text{yr}$ be compared with that of Lyman alpha emitters or faint LBGs. Our simulations suggest that the median $f_{\text{esc},1\text{D}}$ of the sample is 5.1%, which is consistent with $f_{\text{esc},1\text{D}} = 5 - 15\%$ inferred from narrow band filter imaging observations of 91 LAEs (Mostardi et al. 2013). We note that, given the wide distribution of the simulated apparent escape fraction ($0.1\% \lesssim f_{\text{esc},1\text{D}} \lesssim 23\%$ or $0.001\% \lesssim f_{\text{esc},1\text{D}} \lesssim 47\%$ for the

1 and 1.5σ range, respectively), our results are also compatible with the individual detection of LyC fluxes from 7 LBGs (Iwata et al. 2009, $5.5 \lesssim f_{\text{esc},1\text{D}} \lesssim 55\%$ for the intrinsic UV to LyC flux ratio of 3.).

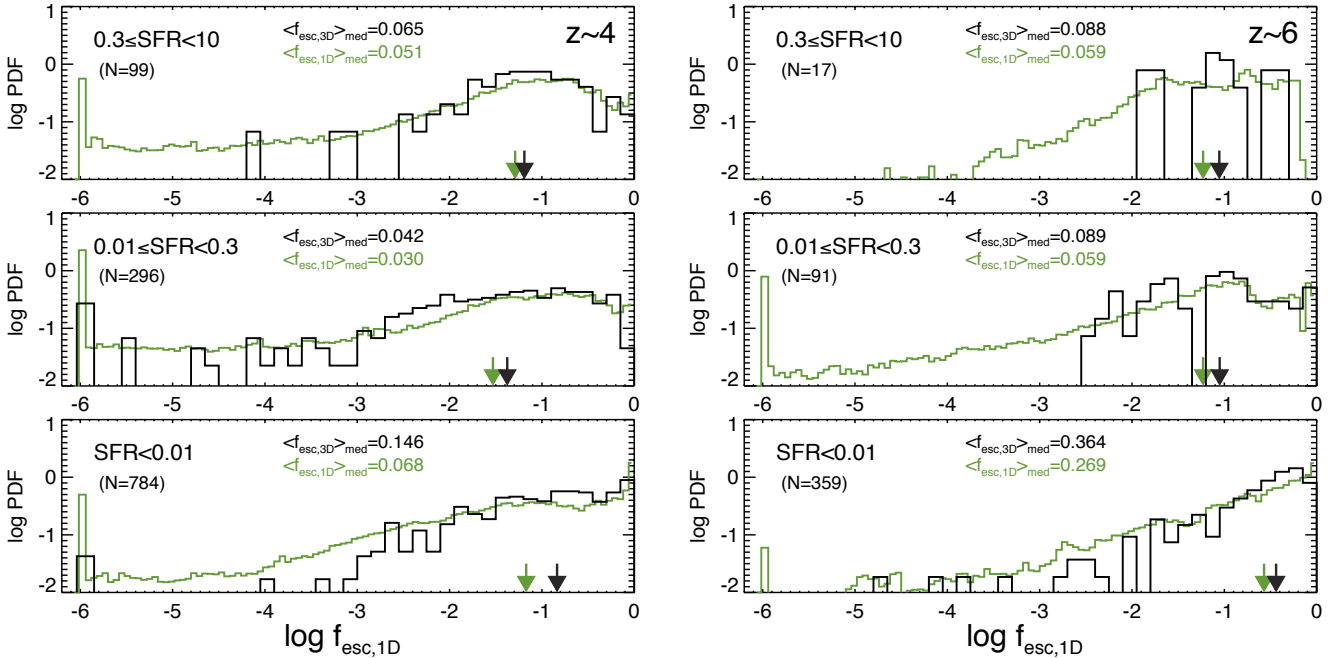


Fig. 3.— is similar to Figure 2, except the galaxy sample is subdivided according to their star formation rates, $\text{SFR}=0.3$ to $10 M_{\odot}/\text{yr}$ (top panel), 0.01 to $0.3 M_{\odot}/\text{yr}$ (middle panel), and $< 0.01 M_{\odot}/\text{yr}$ (bottom panel).

Evidently, the distribution of the apparent LyC escape fraction is very broad and skewed toward the lower end. The reason for this behavior is understandable. In the case of the galaxies with low $f_{\text{esc},3\text{d}}$ values, the LyC photons escape normally through transparent holes with small solid angles. Since not all of these holes are seen to an observer, the distribution of $f_{\text{esc},1\text{d}}$ for individual galaxies tends to get skewed toward the lower end of the distribution. As a result, the medians of the two distributions, shown as arrows in Figure 2, are about a factor of ~ 2 smaller than the mean. More importantly, it suggests that an observational sample of limited size may underestimate the true mean escape fraction. The top two panels of Figure 4 show the probability distribution function of the apparent mean for a given observational sample size N_{stack} for the high mass (top) and low mass (bottom) sample, respectively. We compute the apparent mean of a sample of galaxies using LyC photon (or SFR)-weighted mean escape fraction, which is exactly equivalent to stacking the galaxies. The bottom two panels of Figure 4 are similar to top two panels in Figure 4, for the subsamples with different star formation rates. What we see in these figures is that the probability distribution is rather broad. It is thus clear that it is not a robust exercise to try to infer the mean escape fraction based on a small sample (≤ 10) of galaxies, whether individually measured or through stacking.

Table 1 provides a quantitative assessment of the uncertainties, which shows the 1 and 2σ

probability intervals of fractional lower and upper deviations from the true mean escape fraction. Some relatively mild trends are seen that are consistent with earlier observations of the figures. Specifically, the convergence to the true mean escape fraction in terms of sample sizes is faster towards high redshift, towards higher halo mass, and towards higher star formation rates. Let us take a few numerical examples. We see that with a sample of 50 galaxies of halo mass in the range of $(10^{10} - 10^{11}) M_{\odot}$ at $z = 4$ the 2σ fractional range of the escape fraction is 58% to 159%, which improves to a range of 68% to 140% when a sample of 100 galaxies is used. Note that the observations of Mostardi et al. (2013) have 49 Lyman break galaxies and 91 Lyman alpha emitters at $z \sim 2.85$. At $z = 6$ for the $(10^{10} - 10^{11}) M_{\odot}$ halo mass range, we see that with a sample of 20 galaxies, the 2σ fractional range of the escape fraction is 59% to 161%, comparable to that of a sample of 50 galaxies at $z = 4$, as a result of benefiting from the faster convergence at higher redshift. On the other hand, at $z = 5$ for the $(0.3 - 10) M_{\odot} \text{yr}^{-1}$ star formation rate range, the 2σ fractional range of the escape fraction is 56% to 163% with a sample of 20 galaxies, which is improved to 71% to 137% with a sample of 50 galaxies.

Finally, we note that the actual observed Lyman continuum escape fraction has additionally suffered from possible absorbers in the intergalactic medium, primarily Lyman limit systems. Since the background galaxy and the foreground absorbers are physically unrelated, we may consider the effects from the internal factors in galaxies and those from the intergalactic medium completely independent. Thus, in this case, assuming no knowledge of the foreground absorbers, the overall distribution would be the convolution of the two, resulting a still broader overall distribution than derived above considering internal factors alone. In reality, however, one may be able to remove, to a large degree, the Lyman continuum opacity due to intergalactic absorbers by making use of a tight correlation between Ly α and LyC absorption (Inoue & Kamaya 2008).

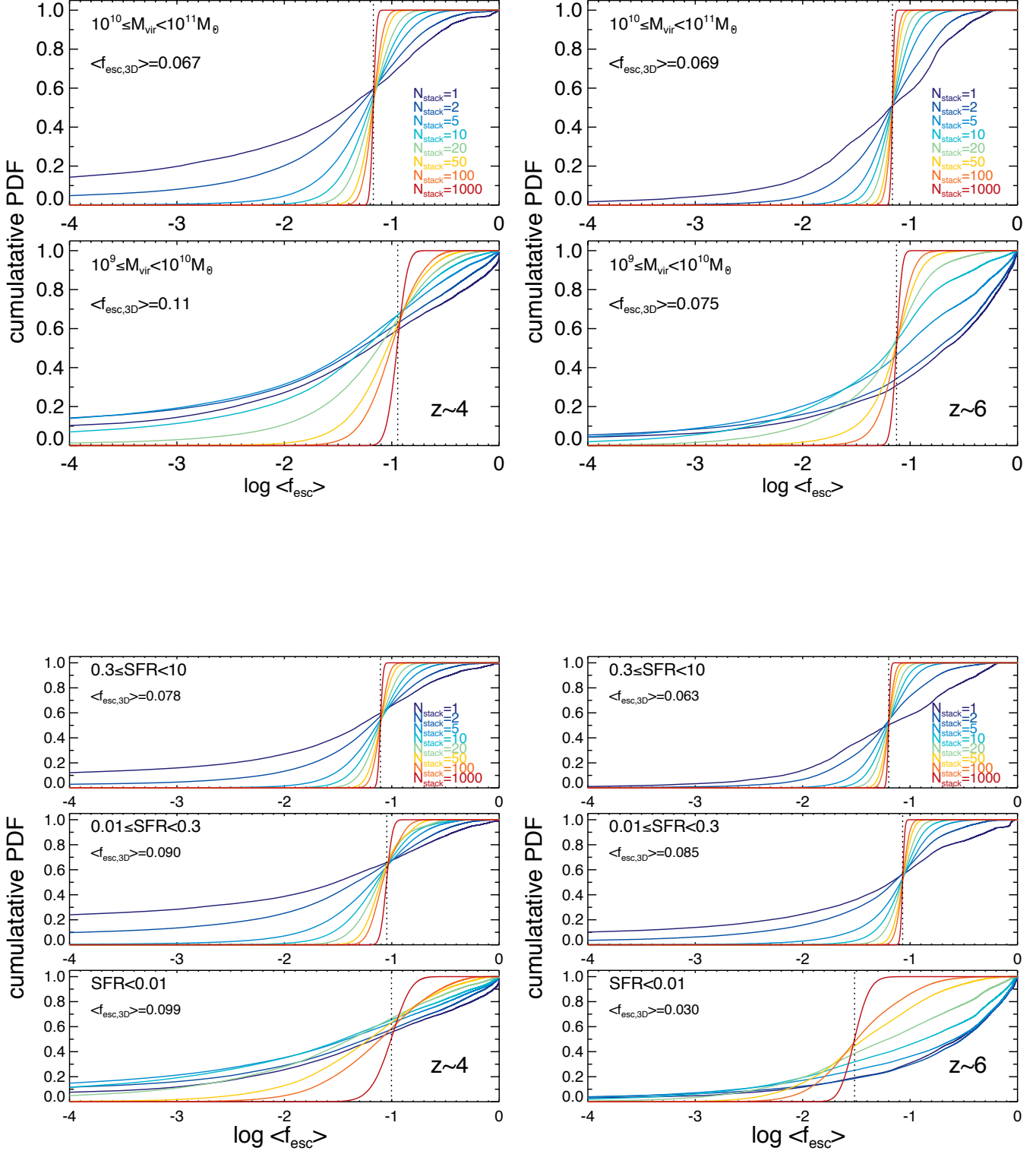


Fig. 4.— **Top two panels** show the probability distribution function of the apparent mean for a given observational sample size N_{stack} for the high mass (top) and low mass (bottom) sample, respectively. The mean is computed by weighting the number of photons produced in each galaxies to mimic the stacking of the SED in observations. The true mean of the distribution is denoted in each panel. **Bottom two panels** are the same as the top two panels, but for the subsamples with different star formation rates, as indicated in the legend.

4. Conclusions

We have simulated a significant sample of galaxies that are resolved at 4 parsec scales, important for capturing the structure of the interstellar medium (e.g., Joung & Mac Low 2006). We have also implemented a much improved supernova feedback method that captures all phases of the Sedov-Taylor explosion solution and has been shown to yield the correct final momentum driven by the explosion regardless of the numerical resolution (Kimm & Cen 2014). An adequate treatment of both these two requirements is imperative, before one can start properly addressing the issue of LyC escape, because most of the escape LyC photons escape through “holes” in the interstellar medium, instead of them uniformly leaking out in a “translucent” medium. In Kimm & Cen (2014) we address the escape fraction for galaxies at the epoch of reionization, to provide the physical basis for stellar reionization.

Here we quantify the distribution of escape fraction for galaxies as a whole, at a range of redshift from $z = 4$ to $z = 6$. In general, it is found that the LyC escape fraction depends strongly on the view angle of the observer and the overall distribution of the escape fraction sampled over many sightlines is very broad. The distribution narrows with increasing halo mass or SFR or redshift. This broad distribution introduces large sampling uncertainties, when the galaxy sample size is limited. For example, a sample of 50 galaxies of halo mass in the range of $(10^{10} - 10^{11}) M_{\odot}$ at $z = 4$ produces the 2σ fractional range of the escape fraction of 58%-159%. At $z = 5$ a sample of 20 galaxies with star formation rate in the range of $(0.3 - 10) M_{\odot}\text{yr}^{-1}$ gives the 2σ fractional range of the escape fraction is 56%-163%. Our analysis suggests that at least on order of tens of galaxies is needed, before one is confident at the 2σ level that the mean escape fraction measured does not deviate from the truth by 30-50% at $z = 4 - 6$ for galaxies hosted by halos of mass in the range $10^{10} - 10^{11} M_{\odot}$.

We thank Rogier Windhorst for useful discussion. Computing resources were in part provided by the NASA High- End Computing (HEC) Program through the NASA Advanced Supercomputing (NAS) Division at Ames Research Center. The research is supported in part by NSF grant AST-1108700 and NASA grant NNX12AF91G.

REFERENCES

- Cen, R. 2003, ApJ, 591, 12
- Cooke, J., Ryan-Weber, E. V., Garel, T., & Gonzalo Diaz, C. 2014, ArXiv e-prints
- Draine, B. T., Dale, D. A., Bendo, G., Gordon, K. D., Smith, J. D. T., Armus, L., Engelbracht, C. W., Helou, G., Kennicutt, Jr., R. C., Li, A., Roussel, H., Walter, F., Calzetti, D., Moustakas, J., Murphy, E. J., Rieke, G. H., Bot, C., Hollenbach, D. J., Sheth, K., & Teplitz, H. I. 2007, ApJ, 663, 866

Table 1: 1 and 2σ ranges of LyC escape fraction in terms of sample size, stellar mass and redshift

	$z = 4$	$z = 5$	$z = 6$
N_{stack}	$(f_{-2\sigma}, f_{-1\sigma}, f_{+1\sigma}, f_{+2\sigma}) / \langle f_{esc} \rangle$	$(f_{-2\sigma}, f_{-1\sigma}, f_{+1\sigma}, f_{+2\sigma}) / \langle f_{esc} \rangle$	$(f_{-2\sigma}, f_{-1\sigma}, f_{+1\sigma}, f_{+2\sigma}) / \langle f_{esc} \rangle$
$10^{10} \leq M_{vir}/M_{\odot} < 10^{11}$			
1	(0.001, 0.004, 3.21, 12.4)	(0.002, 0.097, 4.57, 14.6)	(0.004, 0.162, 3.19, 7.16)
2	(0.001, 0.091, 2.34, 6.14)	(0.011, 0.231, 2.56, 7.45)	(0.092, 0.358, 2.41, 4.58)
5	(0.091, 0.352, 1.81, 3.48)	(0.151, 0.470, 1.87, 3.36)	(0.311, 0.577, 1.65, 2.63)
10	(0.251, 0.509, 1.59, 2.56)	(0.317, 0.601, 1.59, 2.48)	(0.460, 0.682, 1.42, 1.96)
20	(0.405, 0.634, 1.43, 2.02)	(0.470, 0.703, 1.39, 1.92)	(0.588, 0.763, 1.28, 1.61)
50	(0.580, 0.755, 1.27, 1.59)	(0.642, 0.805, 1.24, 1.51)	(0.717, 0.848, 1.17, 1.36)
100	(0.684, 0.823, 1.18, 1.40)	(0.738, 0.859, 1.16, 1.34)	(0.795, 0.889, 1.12, 1.24)
1000	(0.892, 0.942, 1.05, 1.11)	(0.910, 0.951, 1.05, 1.10)	(0.930, 0.965, 1.03, 1.07)
$10^9 \leq M_{vir}/M_{\odot} < 10^{10}$			
1	(0.001, 0.013, 5.37, 8.79)	(0.001, 0.264, 11.0, 13.4)	(0.001, 0.194, 9.98, 13.1)
2	(0.001, 0.003, 3.86, 8.26)	(0.001, 0.155, 10.8, 13.3)	(0.001, 0.132, 9.31, 12.7)
5	(0.001, 0.003, 2.58, 7.38)	(0.001, 0.061, 9.42, 13.0)	(0.001, 0.074, 6.97, 12.3)
10	(0.001, 0.029, 2.03, 5.68)	(0.001, 0.080, 4.87, 12.3)	(0.001, 0.108, 3.05, 10.4)
20	(0.006, 0.151, 1.79, 4.03)	(0.012, 0.185, 2.44, 7.94)	(0.023, 0.231, 1.85, 4.86)
50	(0.131, 0.369, 1.58, 2.97)	(0.134, 0.445, 1.78, 3.23)	(0.170, 0.536, 1.49, 2.33)
100	(0.277, 0.510, 1.49, 2.41)	(0.320, 0.601, 1.52, 2.29)	(0.419, 0.686, 1.33, 1.77)
1000	(0.686, 0.820, 1.18, 1.38)	(0.745, 0.866, 1.14, 1.30)	(0.812, 0.900, 1.10, 1.20)
$0.3 \leq \text{SFR} < 10$			
1	(0.001, 0.014, 2.89, 9.80)	(0.002, 0.106, 3.93, 14.3)	(0.008, 0.185, 4.74, 9.28)
2	(0.001, 0.170, 2.19, 5.18)	(0.005, 0.272, 2.15, 5.53)	(0.062, 0.305, 2.28, 5.49)
5	(0.165, 0.443, 1.76, 3.07)	(0.216, 0.538, 1.62, 2.64)	(0.277, 0.555, 1.58, 2.43)
10	(0.330, 0.583, 1.54, 2.31)	(0.410, 0.666, 1.42, 1.99)	(0.447, 0.672, 1.39, 1.89)
20	(0.476, 0.690, 1.36, 1.84)	(0.562, 0.760, 1.29, 1.63)	(0.583, 0.764, 1.26, 1.58)
50	(0.636, 0.797, 1.23, 1.49)	(0.708, 0.843, 1.17, 1.37)	(0.719, 0.846, 1.16, 1.34)
100	(0.731, 0.853, 1.16, 1.33)	(0.787, 0.888, 1.12, 1.25)	(0.795, 0.890, 1.11, 1.23)
1000	(0.907, 0.953, 1.05, 1.10)	(0.929, 0.964, 1.04, 1.07)	(0.931, 0.963, 1.03, 1.07)
$0.01 \leq \text{SFR} < 0.3$			
1	(0.001, 0.001, 2.87, 8.75)	(0.001, 0.009, 3.74, 12.1)	(0.001, 0.025, 3.99, 10.2)
2	(0.001, 0.023, 2.21, 5.40)	(0.001, 0.108, 2.43, 6.76)	(0.001, 0.121, 2.02, 5.28)
5	(0.034, 0.237, 1.75, 3.70)	(0.098, 0.388, 1.83, 3.23)	(0.100, 0.450, 1.63, 2.87)
10	(0.161, 0.395, 1.52, 3.12)	(0.271, 0.551, 1.58, 2.39)	(0.325, 0.623, 1.42, 2.06)
20	(0.304, 0.515, 1.38, 2.79)	(0.434, 0.669, 1.40, 1.91)	(0.513, 0.731, 1.29, 1.65)
50	(0.468, 0.638, 1.35, 2.10)	(0.605, 0.781, 1.24, 1.53)	(0.684, 0.830, 1.18, 1.38)
100	(0.569, 0.711, 1.32, 1.75)	(0.709, 0.842, 1.17, 1.36)	(0.769, 0.877, 1.13, 1.26)
1000	(0.813, 0.896, 1.10, 1.22)	(0.900, 0.946, 1.05, 1.11)	(0.924, 0.961, 1.04, 1.08)
$\text{SFR} < 0.01$			
1	(0.001, 0.025, 6.95, 10.1)	(0.001, 0.330, 9.99, 12.0)	(0.003, 0.654, 25.5, 32.3)
2	(0.001, 0.009, 5.31, 9.64)	(0.001, 0.263, 10.1, 11.8)	(0.003, 0.674, 25.5, 31.5)
5	(0.001, 0.001, 4.33, 9.36)	(0.001, 0.097, 9.73, 11.7)	(0.003, 0.273, 24.9, 31.1)
10	(0.001, 0.005, 3.66, 9.15)	(0.001, 0.083, 8.51, 11.4)	(0.003, 0.220, 21.3, 30.1)
20	(0.001, 0.025, 2.78, 8.18)	(0.011, 0.124, 4.98, 10.5)	(0.023, 0.246, 14.0, 27.3)
50	(0.015, 0.132, 2.31, 6.04)	(0.054, 0.261, 2.37, 6.66)	(0.095, 0.345, 5.02, 14.8)
100	(0.063, 0.239, 2.20, 4.65)	(0.133, 0.393, 1.96, 4.43)	(0.200, 0.463, 3.00, 7.21)
1000	(0.468, 0.692, 1.38, 1.84)	(0.585, 0.765, 1.28, 1.64)	(0.614, 0.779, 1.30, 1.70)

- Engelbracht, C. W., Rieke, G. H., Gordon, K. D., Smith, J.-D. T., Werner, M. W., Moustakas, J., Willmer, C. N. A., & Vanzi, L. 2008, *ApJ*, 678, 804
- Faucher-Giguère, C., Lidz, A., Hernquist, L., & Zaldarriaga, M. 2008, *ApJ*, 688, 85
- Fisher, D. B., Bolatto, A. D., Herrera-Camus, R., Draine, B. T., Donaldson, J., Walter, F., Sandstrom, K. M., Leroy, A. K., Cannon, J., & Gordon, K. 2013, *ArXiv e-prints*
- Fontanot, F., Cristiani, S., Pfrommer, C., Cupani, G., & Vanzella, E. 2014, *MNRAS*, 438, 2097
- Galametz, M., Madden, S. C., Galliano, F., Hony, S., Bendo, G. J., & Sauvage, M. 2011, *A&A*, 532, A56
- Gnedin, N. Y. 2000, *ApJ*, 535, 530
- Hahn, O., & Abel, T. 2011, *MNRAS*, 415, 2101
- Inoue, A. K., & Kamaya, H. 2008, *ArXiv e-prints*
- Iwata, I., Inoue, A. K., Matsuda, Y., Furusawa, H., Hayashino, T., Kousai, K., Akiyama, M., Yamada, T., Burgarella, D., & Deharveng, J.-M. 2009, *ApJ*, 692, 1287
- Joung, M. K. R., & Mac Low, M. 2006, *ApJ*, 653, 1266
- Kimm, T., & Cen, R. 2014, *ApJ*, 788, 121
- Komatsu, E., Smith, K. M., Dunkley, J., Bennett, C. L., Gold, B., Hinshaw, G., Jarosik, N., Larson, D., Nolta, M. R., Page, L., Spergel, D. N., Halpern, M., Hill, R. S., Kogut, A., Limon, M., Meyer, S. S., Odegard, N., Tucker, G. S., Weiland, J. L., Wollack, E., & Wright, E. L. 2011, *ApJS*, 192, 18
- Leitherer, C., Schaerer, D., Goldader, J. D., Delgado, R. M. G., Robert, C., Kune, D. F., de Mello, D. F., Devost, D., & Heckman, T. M. 1999, *ApJS*, 123, 3
- Lisenfeld, U., & Ferrara, A. 1998, *ApJ*, 496, 145
- Mostardi, R. E., Shapley, A. E., Nestor, D. B., Steidel, C. C., Reddy, N. A., & Trainor, R. F. 2013, *ApJ*, 779, 65
- Nestor, D. B., Shapley, A. E., Kornei, K. A., Steidel, C. C., & Siana, B. 2013, *ApJ*, 765, 47
- Nestor, D. B., Shapley, A. E., Steidel, C. C., & Siana, B. 2011, *ApJ*, 736, 18
- Osterbrock, D. E., & Ferland, G. J. 2006, *Astrophysics of gaseous nebulae and active galactic nuclei*
- Razoumov, A. O., & Sommer-Larsen, J. 2010, *ApJ*, 710, 1239
- Rosdahl, J., Blaizot, J., Aubert, D., Stranex, T., & Teyssier, R. 2013, *ArXiv e-prints*
- Shapley, A. E., Steidel, C. C., Pettini, M., Adelberger, K. L., & Erb, D. K. 2006, *ApJ*, 651, 688

Teyssier, R. 2002, *A&A*, 385, 337

Tweed, D., Devriendt, J., Blaizot, J., Colombi, S., & Slyz, A. 2009, *A&A*, 506, 647

Wise, J. H., & Cen, R. 2009, *ApJ*, 693, 984

Yajima, H., Li, Y., Zhu, Q., Abel, T., Gronwall, C., & Ciardullo, R. 2014, *MNRAS*, 440, 776